SAE TECHNICAL
PAPER SERIES

971640

Use of the Nonlinear Dynamical System Theory to Study Cycle-to-Cycle Variations from Spark Ignition Engine Pressure Data

C.Letellier, S. Meunier-Guttin-Cluzel, and G. Gouesbet
INSA de Rouen

F. Neveu, T. Duverger, and B. Cousyn
PSA Peugeot Citroen

Reprinted from: Diagnostics in SI and Diesel Engines
(SP-1279)

SAE The Engineering Society For Advancing Mobility Land Sea Air and Space.
INTERNATIONAL

International Spring Fuels
& Lubricants Meeting
Dearborn, Michigan
May 5-8, 1997

400 Commonwealth Drive, Warrendale, PA 15096-0001 U.S.A. Tel: (412)776-4841 Fax:(412)776-5760

971640

Use of the Nonlinear Dynamical System Theory to Study Cycle-to-Cycle Variations from Spark Ignition Engine Pressure Data

C.Letellier, S. Meunier-Guttin-Cluzel, and G. Gouesbet
INSA de Rouen

F. Neveu, T. Duverger, and B. Cousyn
PSA Peugeot Citroen

Abstract

Cycle-to-cycle variations in the pressure evolution within the cylinder of a spark ignition engine has long been recognized as a phenomenon of considerable importance. In this work, use of tools borrowed to the nonlinear dynamical system theory to investigate the time evolution of the cylinder pressure is explored. By computing a divergence rate between different pressure cycles versus crank angle, four phases during the combustion cycle are exhibited. These four phases may be identified with the four common phases evidenced by burn rate calculations [1]. Starting from phase portraits and using Poincaré sections, we also study correlations between peak pressures, IMEP and the durations from ignition to appearance of a flame kernel. Accounting for the fact that, during the ignition phase of the combustion cycle, trajectories in a plane projection of the reconstructed phase portrait associated with cycles in the case of motored engine cannot be distinguished from trajectories corresponding to combustion cycles, we estimate the duration of the ignition phase without any prior assumption on the combustion processes. Fluctuations of ignition phase lengths have been found to be correlated with IMEP standard deviations.

1 Introduction

Cycle-to-cycle variations in pressure evolution within the cylinder of a spark ignition engine has long been recognized as a phenomenon of considerable importance [2] [3]. In his monograph [4], Heywood identified three main factors influencing cycle-to-cycle variations (i) aerodynamics in the cylinder during combustion, (ii) the amount of fuel, air and recycled exhaust gases supplied to the cylinder and (iii) the mixture composition, especially near the spark plug. These factors contribute to the cycle-to-cycle variations according to different ways. The aerodynamics of gases and the mixture composition near the spark plug just prior to ignition determine the flame kernel growth during the initiation phase [5]. The way in which the flame front is wrinkled may produce variations in the flame propagation, and consequently, affects the burning rate [6] [7] [8].

The combustion of gases in the cylinder may be viewed as a dynamical system and, by this way, may be studied by tools borrowed to the theory of nonlinear dynamical systems. Indeed, Kantor [9] suggested that the real cause of the variations might be the nonlinear dependence of the peak cycle temperatures and pressures on the initial conditions at the beginning of the cycle due to exhaust gas recirculation. Such nonlinear dependence on initial conditions in other physical systems has been shown to lead to chaotic behaviours [10] [11] [12]. Moreover, a simple spark ignition engine model has been used by Daily [13] to illustrate the concept that cycle-to-cycle variations are an inherent consequence of nonlinear combustion kinetics, and may possibly be connected to a chaotic process. Another simple model was proposed by Daw *et al* [14] to explain the interaction between stochastic, small-scale fluctuations in engine parameters and nonlinear deterministic coupling between successives engine cycles. Consequently, it is appropriate to use techniques pertaining to the dynamical system theory to investigate time evolution of the cylinder pressure to characterize cycle-to-cycle variations.

Such an analysis will start with the first usual step of a dynamical analysis namely the reconstruction of an equivalent state space from the recorded time series. By computing Poincaré sections and first-return maps of the portraits constituted by the trajectories associated with the evolution of the system in the recon-

structed state space, the nature of cycle-to-cycle variations will be investigated. Without prior assumption concerning the combustion processes implied in the evolution of cycles, four phases will be exhibited during the burning process by computing a divergence rate between individual-cycle pressure time evolution. These four phases will be identified with the usual phases defined by burn rate calculations, namely the flame initiation, the flame development, the flame front propagation and the end of combustion. Moreover, accounting for the fact that, during flame initiation, trajectories in a plane projection of the reconstructed phase portrait associated with cycles of motored engine cannot be distinguished from trajectories corresponding to fired cycles, we estimate the length of the flame initiation. Fluctuations of flame initiation lengths have been found to be correlated with IMEP standard deviations.

The paper is organized as follows. Section 2 briefly describes the experiments. In section 3 the state space reconstruction method starting from the pressure data is introduced. The reconstructed trajectory is then analyzed by using Poincaré sections. In section 4, the four phases of combustion are exhibited by computing a divergence rate. A sensitiviy to spark advance is studied in section 5. Section 6 is a conclusion.

2 Experiments

The experiments were carried out with a 2 liters, four strokes, four cylinders port injection spark ignition engine with 2 inlet and exhaust valves per cylinder. The engine was operated under different operating conditions and two different levels of mixture preparation (series II with 20% of EGR), as summarized in TAB. 1. Since this work will rely on an extensive analysis of the cycle-to-cycle pressure variations in the cylinder, let us note that the cylinder pressure was measured by using a QH 32C AVL piezoelectric transducer mounted in the cylinder head of the engine. Also, pressure data were recorded with a step of 1° crank angle, by means of a digital oscilloscope LECROY 9314 L timed by an optical shaft encoder mounted on the engine crankshaft. Data were hereafter transferred to a disk on a SUN computer system for storage and analysis. Cylinder pressure histories were then recorded for a large number of cycles under each operating condition (from 100 up to 400 cycles).

Table 1: *Operating conditions and mixture preparation cases. Series II of measurements is achieved with 20% of EGR.*

Cases	Speed (rpm)	Load L_F (bar)	Equivalence ratio ϕ	Spark advance
I.1	1000	MOTORED ENGINE		
I.2	1000	4.88	1.0	23°
I.3	1000	4.88	0.8	23°
I.4	1000	10.40	1.0	7°
I.5	1600	5.40	1.0	25°
I.6	1200	2.90	0.8	25°
II.1	1000	3.16	1.0	20°
II.2	1000	3.22	1.0	25°
II.3	1000	3.55	1.0	30°
II.4	1000	3.40	1.0	35°
II.5	1000	3.60	1.0	40°
II.6	1000	3.50	1.0	45°

3 State space reconstruction

A state space of a system is defined as a space in which a point corresponds to a completely defined state of the system. The time evolution of the system is therefore associated with a trajectory in the state space. In the case of the combustion of a mixture in a car engine, such a state space is spanned by a certain amount of variables as pressure, temperature, mass fraction of species, ... and many other (uncountable) aerodynamical variables. In our experiments, the time evolution of a single variable is recorded, namely the cylinder pressure $P(t)$. The first step in our dynamical analysis is to reconstruct a state space from this experimental time series $P(t)$. Indeed, it is possible to create a multidimensional space from a scalar time series by using a reconstruction method such as proposed in a pioneering paper by N. H. Packard *et al* [15] by using time delays or time derivatives. Here, the time may ne thought as being the crank angle $\theta(t)$, since this angle just provides an equivalent parametrization. Let us assume that the dimension of the state space associated with the dynamics of our car engine is d_E (or, more loosely, that a state space of dimension d_E can capture proeminent features of the dynamics). Then, we need to reconstruct a space of dimension d_E from the time series $P(t)$. This can be achieved by using the space spanned by the time delay coordinates reading as :

$$\begin{cases} x_1 = P(t) \\ x_2 = P(t+\tau) \\ \vdots \\ x_{d_E} = P(t+(d_E-1)\tau) \end{cases} \quad (1)$$

where τ is a time delay to be evaluated (see [16] for a review concerning this evaluation) or, alternatively, by using derivative coordinates :

$$\begin{cases} x_1 = P(t) \\ x_2 = \dfrac{dP(t)}{dt} = \dot{P}(t) \\ \vdots \\ x_{d_E} = \dfrac{d^{d_E-1}P(t)}{dt^{d_E-1}} \end{cases} \quad (2)$$

Another kind of coordinates, namely principal components [17], is also currently used in the analysis of dynamical systems. J. F. Gibson *et al* [18] demonstrated that the relationship between delays, derivatives and principal components consists on a rotation and a rescaling. Consequently, from Gibson's point of view, statements about a dynamics observed in a reconstructed state space would not depend on the coordinates. Nevertheless, they may depend on reconstruction parameters such as the time delay τ, the sampling rate δt or the window size τ_w on which the derivatives are computed.

In this paper, we prefer to use derivative coordinates for two reasons (i) the shape of the reconstructed state portrait, i.e. the trajectory associated with the time evolution of the engine, is less sensitive to the choice of the window size τ_w used in computing derivatives than to the choice of the time delay τ introduced in the delay coordinates and (ii) derivatives (in particular the first derivative $\dot{P}(t)$) possess an obvious physical meaning. The derivatives are here estimated by using a discrete linear filter

$$w_j(t) = \sum_{n=-p}^{p} r_{j,p}(n)x(t+n\delta t) \quad (3)$$

where the time series $x(t)$ (here pressure versus time) discretized with the time step δt is the input, $w_j(t)$, the so-called Legendre coordinate, is the output, and $r_{j,p}(n)$ is an appropriate discrete convolution kernel, namely constituted of the discrete Legendre polynomials, parametrized by the choice of p which defines the window size $\tau_w = (2p+1)\delta t$ and the order j of the required derivative. Following Gibson *et al* [18], this filter defines the optimal linear coordinate transformation.

In this work, most of the analysis is achieved by working in a plane projection of the reconstructed state space, i.e. by working in a plane spanned by $P(t)$ and $\dot{P}(t)$. A few tasks such as computing the Poincaré sections are carried out by working in a 3D space where the third coordinate is $\ddot{P}(t)$.

For instance, parts of time series and plane projections of reconstructed state spaces are given for three different operating conditions (Figure 1). In each case, a single trajectory associated with about ten successive cycles is displayed. In this paper, the word cycle will designate either a cycle of combustion or the part of the trajectory associated with a cycle of combustion. The case of motored engine is displayed in Figure 1.a. As expected, the trajectory is well transversely confined in the state space. This is the obvious result of the very small dispersion of the cylinder pressure cycle when there is no combustion during the cycle. From this point of view, the cylinder pressure, which is a macroscopic variable, is fairly insensitive to the aerodynamics of the mixture. Two cases of combustion are displayed in Figure s 1.b and 1.c. The first one is for an equivalence ratio ϕ equal to 1 (case I.2. Figure 1.b) and the second one is for $\phi = 0.8$ (case I.3, Figure 1.c). When $\phi = 1.0$, the trajectory moderately fluctuates around a mean orbit in concordance with the small relative standard deviation of IMEP ($COV_{\text{IMEP}} = 1.8\%$). With a leaner equivalence ratio (Figure 1.c), the trajectory visits a larger region of the state space as expected from the greater magnitude of IMEP variations ($COV_{\text{IMEP}} = 7.6\%$).

The state portraits allow us to easily distinguish dynamics with different operating conditions. In any case, trajectories are rather well confined in the state space and well organized, i.e. different cycles are associated with parts of trajectory which are nearly parallel. Consequently, cylinder pressure evolution could be possibly governed by a dynamics with a deterministic component. We then invoke the theory of dynamical systems which tells us that, when a dynamics is governed by a low-dimensional deterministic process, i.e. is associated with a small number of ordinary differential equations, the dynamics must induce a first-return map which exhibits a structure. By structure, we here mean a repartition which is different fom a cloud of points as would be obtained in the presence of a stochastic behaviour. Therefore, a first-return map is now computed in a Poincaré section which is here defined as :

$$P = \{(X,Z) \in \mathbb{R}^2 \mid Y = 0, Z < 0\} \quad (4)$$

where

$$\begin{cases} X = P(t) \\ Y = \dot{P}(t) \\ Z = \ddot{P}(t) \end{cases} \quad (5)$$

Such a Poincaré section is displayed in Figure 2 (for case I.2). From this Poincaré section, a first-return map is computed by plotting the coordinate X_{n+1} of the $(n+1)$-th intersection between the trajectory and the Poincaré section versus the coordinate X_n of the n-th intersection. This first-return map is displayed in Figure 3. It exhibits a structure similar to a cloud of points meaning that cycle-to-cycle variations of the cylinder pressure are not only governed by a low-dimensional deterministic dynamics. It is then highly likely that the dynamics of the cylinder pressure has a deterministic component associated with the global shape of a cycle and a stochastic component describing the cycle-to-cycle variations. Consequently, it would be reasonable to assume that cycle-to-cycle variations are not governed by a chaotic process since a stochastic component is exhibited.

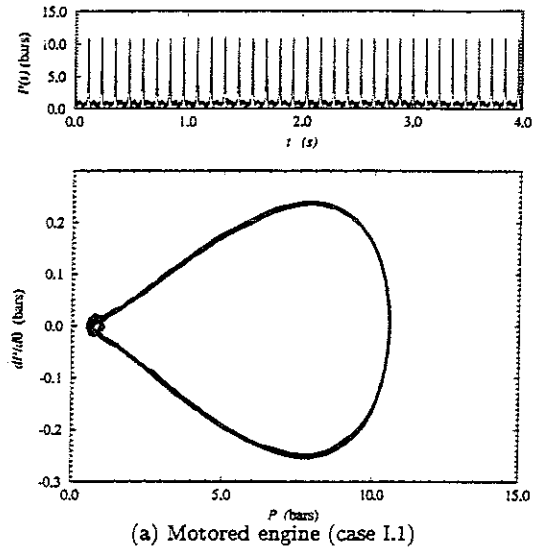

(a) Motored engine (case I.1)

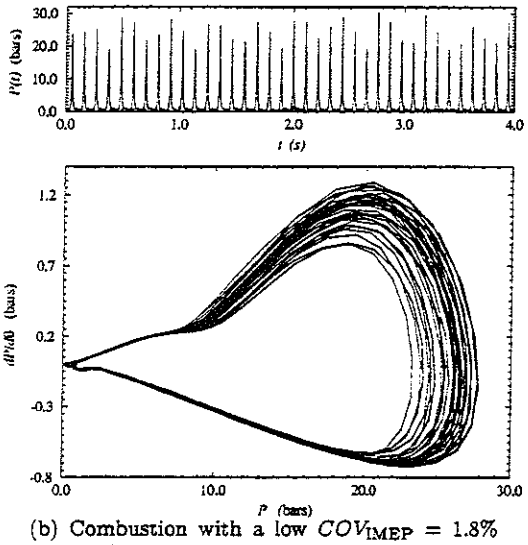

(b) Combustion with a low $COV_{\mathrm{IMEP}} = 1.8\%$ (case I.2)

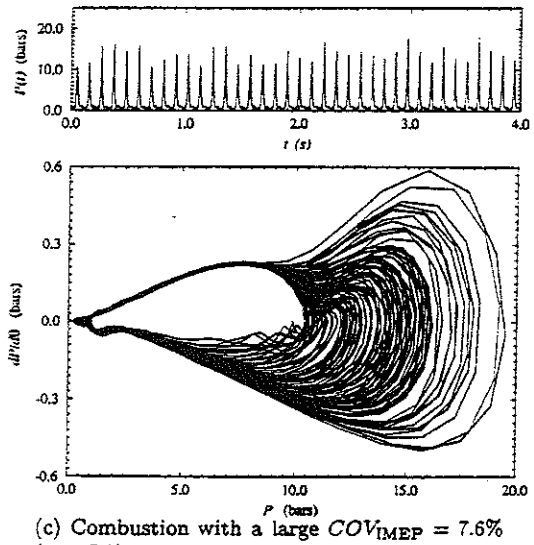

(c) Combustion with a large $COV_{\mathrm{IMEP}} = 7.6\%$ (case I.3)

Figure 1: *Parts of the recorded time series with plane projections of reconstructed state spaces for three operating conditions. The relative standard deviation of IMEP is indicated when required.*

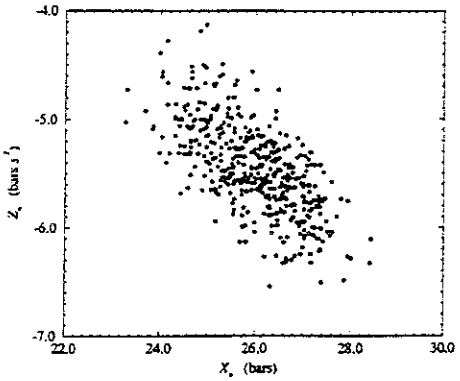

Figure 2: *Poincaré section P computed for case I.2.*

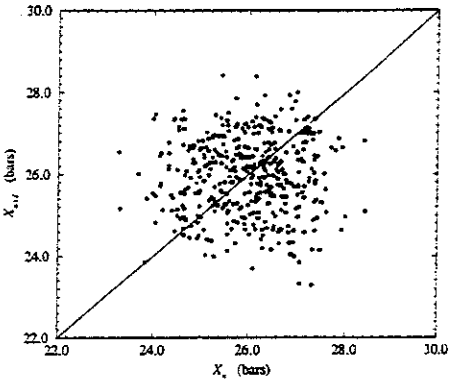

Figure 3: *First-return map to the Poincaré section P (case I.2).*

4 Divergence rate and burning events

One of the common techniques of analysis of the dynamical behaviour of engines is constituted by using a mass-fraction-burned calculation versus crank angle θ. During a cycle, the burning process is then usually separated in four phases [1] as follows (i) the flame initiation associated with the angular range corresponding to a burned mass fraction (BMF) up to 2%. During this phase, the burning process is not detected by analyzing the cylinder pressure (ii) the flame development associated with burned mass fractions in the range $2\% \leq \mathrm{BMF} \leq 10\%$. The flame kernel becomes a flame front during this phase (iii) the flame propagation, corresponding to the propagation of a flame front from the ignition site through the combustion chamber, arises when $10\% \leq \mathrm{BMF} \leq 90\%$. (iv) the end of the combustion which is completed when $\mathrm{BMF} = 100\%$.

The beginning of the combustion process is easily identified since it is associated with the spark ignition angle, expressed as a spark advance SA (in degrees) before the Top Dead Center (TDC). In our experiments, no significative difference in pressure evolution has been observed in both fired and cycles of motored engine before the spark ignition angle θ_{init}, in spite of possible changes

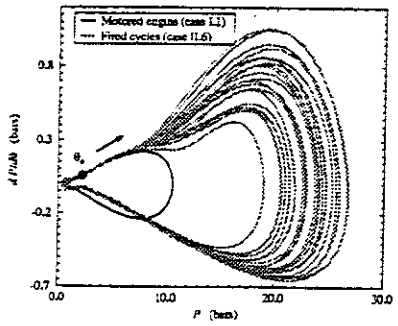

Figure 4: *Comparison between plane projections of the trajectories associated with fired cycles and cycles of motored engine.*

due to residual gases whose temperature may change the specific ratio $\gamma = \frac{C_p}{C_v}$ of the unburned mixture. This fact may be observed in Figure 4 where the trajectory associated with cycles of motored engine essentially coincides, in the same plane projection of the reconstructed state space, with the trajectory corresponding to fired cycles. Fired trajectories and motored engine trajectories differently evolve after a short time delay beyond the spark ignition. One has to remark that, due to the influence of different thermodynamical conditions (pression, temperature, mass fractions, ...), the trajectories for motored engine and fired cycles are very different at the end of the cycles, even after the completion of the combustion. This is a signature of the influence of the thermodynamical conditions which are, of course, different depending on whether combustion occurred or not.

Just after the spark ignition, fired trajectories separate from motored engine trajectories due to the cylinder pressure increase induced by the flame development. Associated to this difference between the behaviour of the two kinds of cycles, there also occurs a difference of behaviour between fired cycles. However, the fired cycles eventually converge toward the same evolution once the burned gases are ejected from the cylinder. We may expect that the burning phase corresponds to the interval defined by the onsets of divergent and convergent behaviours.

These behaviours may allow to identify the roots of the cyclic dispersion without any prior knowledge about combustion processes. This may be done by exhibiting critical angles associeated with the different burning events appearing during a cycle by computing a divergence rate λ_θ from the pressure time series. This divergence rate λ_θ is adapted from the Lyapounov exponent definition [19] to our data and is then defined as follows :

$$\lambda_\theta \approx \frac{1}{N!} \sum_{i=1}^{N-1} \sum_{j=i+1}^{N} \log \frac{|X_{\theta+\delta\theta}(i) - X_{\theta+\delta\theta}(j)|}{|X_\theta(i) - X_\theta(j)|} \quad (6)$$

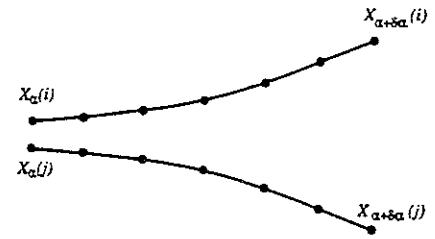

Figure 5: *Evolution of the distance between two cycles versus crank angle. Here, the angle delay is taken to be equal to 6°.*

where $X_\theta(i)$ designates the pressure value at angle θ during the i-th cycle, δ_θ is an angle delay on which the divergence rate is estimated (see Figure 5) and N is the number of cycles on which the divergence rate is estimated. In spirit, this divergence rate is similar to a local Lyapounov exponent in nonlinear dynamics and may therefore be called a Lyapounov index.

The angle delay is empirically set to 6°. For an angle delay smaller than 6°, parasitic oscillations appear in the evaluation of λ_θ (noise corruption). This value of 6° is the smallest value for which these parasitic oscillations are no more disturbing. The evolution of the divergence rate is displayed in Figure 6 for motored engine and fired cycles.

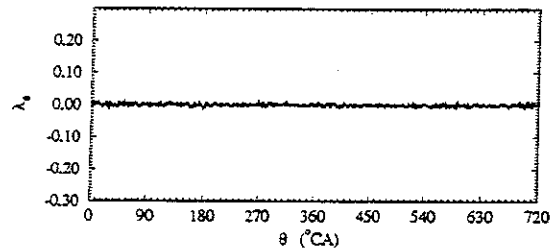

(a) Motored engine (case I.1)

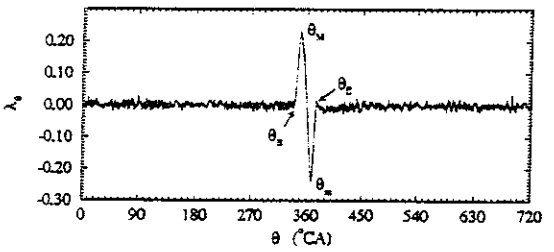

(b) Fired cycles (case I.2)

Figure 6: *Divergence rate λ_θ versus crank angle for two different operating conditions. λ_θ is computed over about 300 cycles.*

Table 2: *Critical crank angles for some operating conditions. Values of IMEP are also reported.*

case	θ_{init}	θ_B	θ_M	θ_m	θ_E	IMEP
I.3	337^o	342^o	356^o	390^o	418^o	2.85
I.6	335^o	342^o	353^o	391^o	417^o	3.19
I.2	337^o	337^o	349^o	367^o	375^o	6.91
I.4	353^o	350^o	360^o	378^o	386^o	3.99
I.5	335^o	337^o	348^o	367^o	376^o	4.37

As expected, the divergence rate λ_θ is about zero on the interval $[0^o - 720^o]$ for cycles of motored engine. This means that no divergence (convergence) appears during cycles, in concordance with the fact that the cycle-to-cycle dispersion is very small and may be viewed as resulting from the corruption of data by noise. Conversely, when there is combustion during cycles, a significant cycle-to-cycle dispersion appears as evidenced by the large two-peak oscillation of the divergence rate λ_θ (Figure 6.b). From the structure of this oscillation, four critical crank angles may be defined (i) the crank angle θ_B corresponding to the beginning of the oscillation (ii) the angle θ_M for which λ_θ reaches its maximum value, (iii) θ_m defining the minimum value of λ_θ and (iv) θ_E which is associated with the end of the oscillation. The values of these different critical angles for a few operating conditions are reported in Table 2.

We recall now that our main objective is to exhibit useful tools arising from the nonlinear dynamical theory to analyse cylinder pressure time series without any prior knowledge on combustion processes. Such a goal is motivated by the very cumbersome character of the burn rate calculation codes which are more classically used. Indeed, to obtain good results with such codes, many physical parameters (wall temperature, piston temperature, natural EGR rate, ...) must be adjusted. Moreover, it is not always well understood how a small change in one of these control parameter values acts on the results. A complete study of the results given by such a code over a large range of the control parameter values would be useful. Nevertheless, such a study is out of the scope of this paper and is therefore postponed to a future work. But let us provide an exemplifying comparison between results of a conventional heat release code and results given by computing a divergence rate. We have to precise that, in this preliminary comparison, control parameter values are not necessarily carefully adjusted. Results are reported in Table 3.

From the results obtained with such a conventional heat release analysis, we may observe that 12^o after the spark ignition, only 1.3% of the mass are burned which is a very small value for a stochiometric mixture. Nevertheless, quantitative results allows us to assume that

Table 3: *Comparison between nominal values of BMF following our assumptions concerning the interpretation of the divergence rate and the computed values by using a conventional Heat Release Analysis (HRA). Nominal values of BMF are associated with the usual four phases during the combustion cycle.*

$\Phi = 1.0$ case I.2				
BMF	2 %	10 %	90 %	100 %
λ_θ	$\theta_B =$ 337^o	$\theta_M =$ 349^o	$\theta_m =$ 367^o	$\theta_E =$ 375^o
HRA	0.0 %	1.3 %	58.5 %	90.0 %
σ_{BMF}	-	0.5 %	10.5 %	3.9 %
$\Phi = 0.8$ case I.3				
BMF	2 %	10 %	90 %	100 %
λ_θ	$\theta_B =$ 342^o	$\theta_M =$ 356^o	$\theta_m =$ 390^o	$\theta_E =$ 418^o
HRA	0.6 %	2.7 %	71.6 %	96.7 %
σ_{BMF}	0.4	1.0 %	16.6 %	4.7 %

critical crank angles may be used to interpret the combustion cycle as follows.

By inspecting the critical crank angle values, one may remark that the oscillation starts a short time after the spark ignition. The interval $(\theta_B - \theta_{init})$ may therefore be associated with the flame initiation since, during this phase, the cylinder pressure is not sensitively affected by the combustion. More generally, it is worth stating at this point that four phases are again distinguished by the divergence rate in the burning angular range. Indeed, the oscillation is divided in three intervals separated by the critical crank angles to which we must add the interval $(\theta_B - \theta_{init})$. It then appears that each interval of the oscillation would correspond to a phase of the burning process. Then, the flame development can be defined by the interval $[\theta_B, \theta_M]$, the propagation by the interval $[\theta_M, \theta_m]$ and the end of the combustion by the interval $[\theta_m, \theta_E]$. With such an identification, the mean angular range associated with each phase of the burning process may be determined (Table 4).

From these results, we check that the flame initiation depends on the equivalence ratio of the mixture, i.e. the flame initiation angular range increases when ϕ decreases ($< 1^o$ when $\phi = 1.0$ and $5^o - 7^o$ when $\phi = 0.8$). Such a result is in agreement with the well known fact that the initiation of a flame kernel near the spark plug is faster with a stochiometric operating condition than with leaner equivalence ratios. For a given equivalence ratio however, the angular ranges associated with the different phases of combustion are not sensitively affected by the operating conditions. Nevertheless, the different loads applied to the engine and the different spark timing modify the IMEP values. Also, the flame development range (equal to about ten degrees in each

Table 4: *Intervals associated with the different phases of the burning process estimated by the critical crank angles. The relative standard deviation of IMEP is also reported.*

case	Init.	Dev.	Prop.	End	Tot.	COV_{IMEP}
I.3	5°	14°	34°	28°	76°	7.6 %
I.6	7°	11°	38°	26°	75°	11.4 %
I.2	< 1°	12°	18°	8°	38°	1.2 %
I.4	< 1°	10°	18°	8°	36°	1.8 %
I.5	2°	11°	19°	9°	39°	1.8 %

case) appears to be rather insensitive to the operating conditions, including the equivalence ratio. Furthermore, the flame propagation range is twice longer when $\phi = 0.8$ than when $\phi = 1.0$ as previously observed [20]. Table 4 also shows that the higher the flame speed is, the smaller is the cycle-to-cycle dispersion as indicated by the relative standard deviation COV_{IMEP}. Such a result has been experimentally observed by Young [21] and numerically by Daily [13] with a simple model. The range of the end of combustion also appears to depend much on the equivalence ratio. As a conclusion to this section, we mention then that the characterization of the different phases of the burning process by the divergence rate λ_θ is in agreement with the usual observations, i.e. one might reasonably claim that the different phases of combustion are well determined by the divergence rate λ_θ.

5 Sensitivity to spark advance

Our aim is now to test the sensitivity of the divergence rate λ_θ to the spark timing, and in particular to investigate the evolution of the different phases of combustion versus the spark timing. In order to extend the range of the spark interval without knock, the engine is operated with 20% of EGR. The spark timing is then varied on the range $[20° - 45°]$ (see Table 1). For each spark advance value, the divergence rate λ_θ, IMEP and relative standard deviation of IMEP are computed. Results are reported in Table 5 and Table 6. There is no significant effect of the spark advance on the duration of the combustion phases excepted for the flame initiation phase which occurs on a larger angular range when the spark advance increases. This modification of the flame initiation however does not necessarily degrade the quality of combustion since, as we shall see later, the optimal phasing of the combustion events which produces the highest IMEP is obtained with $SA = 40°$ (with a flame initiation developing over 15°). Again, the flame development angular range is found to be equal to about ten degrees, confirming the absence of dependence on operating conditions found in the previous section for this feature. For the engine used in this work, the optimal phasing is found to correspond to a spark ignition located at 40° before TDC and is associated with the value of COV_{IMEP}.

Table 5: *Different phases of combustion versus the spark advance.*

Cases	AA	Init.	Dev.	Prop.	End
II.1	20°	6°	12°	32°	13°
II.2	25°	8°	10°	30°	13°
II.3	30°	9°	13°	30°	18°
II.4	35°	12°	13°	27°	14°
II.5	40°	15°	13°	27°	12°
II.6	45°	17°	15°	26°	13°

It is not possible to obtain the angular range of flame initiation in individual cycles by using the divergence rate λ_θ, since this last quantity is a statistical quantity. Nevertheless, as a possible correlation between flame initiation durations and IMEP would be of importance, we use directly the plane projections in the reconstructed space to estimate individual initiation phase durations. Then, starting from the fact that, during the flame initiation, the burning process does not significantly affect the cylinder pressure, we define the end of the flame initiation when motored engine trajectories are separated from the cycle-fired trajectory under study by a distance greater than a critical distance d_c for the corresponding plane projection in the reconstructed state space. By this way, an estimation of the flame initiation angular range is obtained for each cycle. In order to prevent our estimation from noise corruption, the distance d_c is set to a big enough value, namely 1.0 (with pressures taken in bars). Such a criterion differs slightly from a departure of 1 bar cylinder pressure cycle in the sense that it is a distance in a 2D space. Moreover, derivatives imply a small smoothing of the data and, consequently, help us to prevent our estimation from noise corruption. For each spark advance value, we then compute the mean value of the initiation angular range δ_I and its associated standard deviation σ_{δ_I}. Results are reported in Table 6.

Due to the use of a relatively large critical distance d_c, the initiation phase is a little bit overestimated. This may be observed by comparing (in Table 6) δ_I values and the flame initiation angular ranges obtained by using the divergence rate λ_θ given also in Table 5. Nevertheless, both evaluations of the flame initiation angular ranges exhibit a similar evolution with respect to the spark advance. The standard deviation σ_{δ_I} of individual-cycle flame initiation angular ranges is also

Table 6: *Estimation of the flame initiation angular ranges and of associated standard deviation by using plane projections in the reconstructed space.*

Series	Init.	δ_I	σ_{δ_I}	IMEP	COV_{IMEP}
II.1	6°	9.0°	18.2	3.806	5.6
II.2	8°	13.0°	15.9	3.801	4.1
II.3	9°	16.1°	11.8	3.846	2.8
II.4	12°	18.7°	9.9	3.949	1.8
II.5	15°	22.1°	10.4	3.955	1.6
II.6	17°	25.9°	11.1	3.950	1.7

computed. This standard deviation σ_{δ_I} is found to decrease as does COV_{IMEP}. In order to evidence a correlation between both quantities, COV_{IMEP} is plotted versus the standard deviation σ_{δ_I} of the flame initiation angular range (Figure 7). As displayed in Figure 7, COV_{IMEP} is nearly linearly related to σ_{δ_I}. Therefore, the variations in the flame initiation range angle affect IMEP variations. This result makes sense since the variations of the flame initiation angular range directly affect the phasing of the combustion process relatively to the piston motion. The largest IMEP for case II.5 (Table 5) corresponds to the smallest COV_{IMEP} and to a spark advance of 40° (Table 1). This particular value of 40° corresponds to the Maximum Brake Torque (MBT) for which any fluctuation in early combustion will have less influence. One conclusion is that the flame development likely does not play a significant role in the cycle-to-cycle dispersion, in so far as it is essentially constant (about ten degrees), irrespective of the operating conditions. Also, the high correlation between COV_{IMEP} and σ_{δ_I} indicates a preponderant role of the initiation phase on cycle-to-cycle variations.

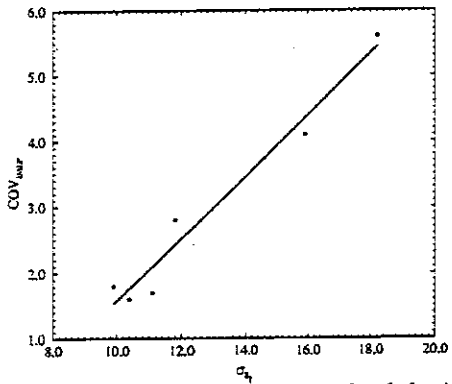

Figure 7: *Correlation between the standard deviation of the flame initiation angular range and COV_{IMEP}.*

Let us now return to the state portraits displayed in Figure 1. We may then remark that a few degrees after the spark ignition, the different individual cycles are separated by the divergence of the dynamical evolution of the cylinder pressure, due to the burning process. The fact that the burning process induces cycle-to-cycle variations has also been evidenced by using the divergence rate λ_θ. Later on, portions of the trajectory associated with different cycles flow rather parallely (before the appearance of a converging behaviour). This property is a signature of a deterministic behaviour (not sensitive to initial conditions, i.e. not chaotic) since a given initial condition allows to predict fairly well the next values of P and $\dot{P}$ during the same cycle. Of course, it is here understood that initial conditions are taken after the end of the flame initiation range, i.e. after that the burning process started to significantly affect the cylinder pressure and that the dispersion of the individual cycles in the trajectory begun.

It is also found that the flame initiation angular range is fairly linearly related to the maximum pressure value reached during a cycle when the flame initiation angles range into the interval $[10° - 20°]$ (Figure 8). When the flame initiation takes too long a time (δ_I greater than 20°), the combustion efficiency is quickly degraded by a decompression effect which is not favourable to the flame front propagation. In this case, the maximum cylinder pressure value is about equal to the maximum pressure value reached during cycles motored engine.

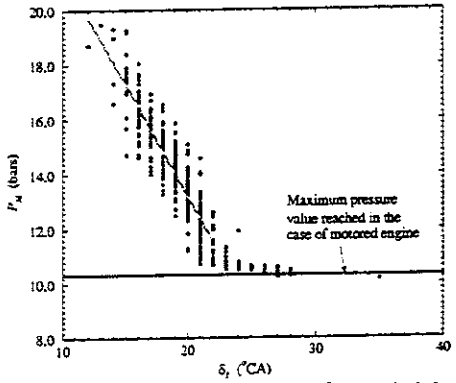

Figure 8: *Correlation between the flame initiation angular range and the maximum cylinder-pressure value P_M. (case I.3)*

To end this study, we now investigate the relationship between IMEP and the flame initiation angular range δ_I for two different equivalence ratios. Individual-cycle IMEP values are plotted versus the flame initiation angular range δ_I for $\phi = 1.0$ (case I.2) and for $\phi = 0.8$ (case I.3) (Figure 9). When the equivalence ratio is equal to 1, the variations in cycle phasing are too small (in concordance with a small value of the standard deviation of the flame initiation angular range) to significantly affect IMEP values (Figure 9.a). Indeed, it is usually claimed that IMEP is unsensitive to cycle phasing around TDC. Conversely, with a leaner equivalence ratio, the duration of the combustion process is longer, allowing the mixture inhomogeneities to have a significant effect on the combustion quality. Large variations in the flame

initiation angular range therefore appear. IMEP values are then clearly affected (Figure 9.b), i.e. a strong correlation appears between IMEP and δ_I. A quadratic regression is computed for this correlation, reading as :

$$\text{IMEP} = A_0 + A_1\delta_I + A_2\delta_I^2 \qquad (7)$$

with

$$\begin{cases} A_0 = 1.8813 \\ A_1 = 0.1672 \\ A_2 = -0.0055 \end{cases}$$

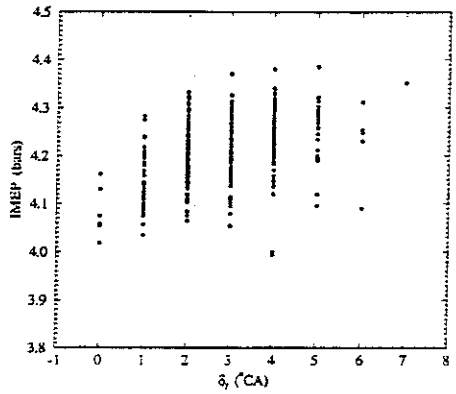

(a) Case I.2 :$\theta_{init} = 23°$, $\phi = 1.0$

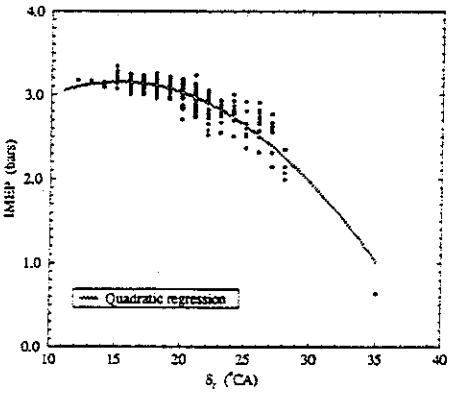

(b) Case I.3 :$\theta_{init} = 23°$, $\phi = 0.8$

Figure 9: *Correlation between the flame initiation angular range and IMEP values for two equivalence ratios.*

This correlation essentially means that the longer the flame initiation angular range is, the smaller IMEP values are. Due to the small value of A_2, IMEP is about linearly related to the flame initiation angular range for small values of δ_I, say when δ_I is smaller than 20°. Furthermore, up to this value of 20°, the cycle phasing is close to the optimal phasing and combustion events are not affected (i.e. IMEP remains actually fairly constant). Beyond this value, the quadratic term becomes significant and a significant decrease of IMEP is observed. Several physical explanations for this decrease could be given. One of them is that, when the flame initiation angular range exceeds 20°, the flame could propagate in the combustion chamber significantly after the minimum cylinder volume is reached. Therefore, the increase in pressure and temperature is less significant since the decompression has begun. Moreover, in this case, it is possible that the flame propagation be sensitive to aerodynamics, implying a slight increase of the fluctuations of IMEP for large flame initiation angular ranges (see Figure 9).

Conversely, the smaller fluctuations of IMEP observed when δ_I is small (case I.2 as well as case I.3 when $\delta_I < 20°$) suggest that, when the cycle phasing is optimal, combustion events are less sensitive to the aerodynamics. In other words, when the cycle phasing is optimal, the flame propagation starts before TDC and the conditions of temperature and pressure are then favourable to the combustion. In such a situation, the flame propagation occurs, on average, independently from the aerodynamics or mixture nonhomogeneities.

6 Conclusion

Cycle-to-cycle combustion variability and how it is influenced by flame initiation was studied in a four-cylinder spark ignition engine. By using tools borrowed to the theory of nonlinear dynamical systems, namely state space reconstruction, Poincaré section and first-return map, it is found that the cycle-to-cycle cylinder pressure variations are not governed by a chaotic process, in the sense that cycle-to-cycle variations are found to be the combination of a non chaotic deterministic component and of a stochastic component. As a consequence, the overall behaviour of the engine cannot be described as a low-dimensional deterministic dynamics but rather, as suggested by Daw *et al* [14], by a superimposition of a nonlinear low-deterministic dynamics with a stochastic component.

By relying on the evaluation of a divergence rate, the flame initiation duration has been found to be related to the maximum cylinder pressure reached during cycles, but not necessarily related to IMEP. Such a result is actually not very surprising since IMEP values are particularly sensitive to cycle phasing of the burning events. Conversely, the relative standard deviation of the flame initiation angular range is linearly related to the standard deviation of IMEP. The earlier events of combustion therefore play a relevant role in cycle-to-cycle variations. This assertion is validated by the fact that trajectories are locally parallel during combustion cycles. Such a property may be viewed as a signature that no stochastic fluctuations appear during the remaining part of the combustion cycle. This conclusion is particularly true in the case of leaner equivalence ratios. Indeed, it is known that mixture nonhomogeneities play a significant role in the case of leaner equivalence ratios for which the stability of the combustion is lower, as

exemplified by the large flame initiation duration found with a small equivalence ratio. Following our assumptions concerning the divergence rate interpretation, for a given equivalence ratio, it is found that the angular ranges of the combustion events are rather insensitive to the operating conditions. Moreover, the flame development is found to be insensitive to the value of the equivalence ratio. These conclusions remain to be validated by a careful comparison with a conventional heat release analysis which is postponed to future works.

Acknowledgements
We wish to thank M. Trinité, J. Reboux and F. Dionnet for their helpful discussions.

References

[1] **M. L. Szenderowicz & J. B. Heywood.** Mixture nonuniformity effects on S.I. engine combustion variability, *SAE Technical Papers Series*, 902142, 1990.

[2] **D. J. Patterson.** Cylinder pressure variations : a fundamental combustion problem, *SAE Technical Paper Series*, 660129, 1966.

[3] **R. K. Barton, D. K. Kenemuth, S. S. Lestz, W. E. Meyer.** Cycle-to-cycle variations of a spark ingnition engine - a statistical analysis, *SAE Technical Paper Series*, 700488, 1970.

[4] **J. B. Heywood.** Internal combustion engine fundamentals, MacGraw-Hill, 1988.

[5] **M. Lebel, M. J. Cottereau.** Study of the effect of the residual gaz fraction on combustion in a S.I. engine using simultaneous CARS measurements of temperature and CO_2 concentration, *SAE Technical Paper Series*, 922388, 1992.

[6] **F. Zhao, T. Kadota, T. Takemoto.** Mixture strength measurements in the combustion chamber of S. I. Engine via Rayleigh scattering, *JSME* Serie II, 35 (4), 1992.

[7] **J. Meyer, M. Harry, M. Schreiber, S. Unverzagt.** Controlling combustion in a spark ignition engine by quantitative fuel distribution, *SAE Technical Paper Series*, 950107, 1995.

[8] **J. Reboux, D. Puechberty, F. Dionnet.** Influence of the injection configuration on mixture preparation and combustion development in a S. I. engine using laser induced fluorescence, *SAE Technical Paper Series*, 961205, 1996.

[9] **J. C. Kantor.** A dynamical instability of spark ignition engines, *Science*, 224, 1233, 1984.

[10] **C. Letellier, L. Le Sceller, P. Dutertre, G. Gouesbet, Z. Fei, J. L. Hudson** Topological characterization and global vector field reconstruction from experimental electrochemical system, *Journal of Physical Chemistry*, 99, 7016-7027, 1995.

[11] **C. Letellier, G. Gouesbet, F. Soufi, J. R. Buchler, Z. Kolláth.** Chaos in variable stars : topological analysis of W Vir model pulsations, *Chaos*, 6 (3), 466-476, 1996.

[12] **C. Letellier, G. Gouesbet, N. Rulkov.** Topological analysis of chaos in equivariant electronic circuits, *International Journal of Bifurcation & Chaos*, 6 (12), December 1996.

[13] **J. W. Daily.** Cycle-to-cycle variations : a chaotic process ?, *Combustion Science and Technology*, 57, 149-162, 1988.

[14] **C. S. Daw, C. E. Finney, J. B. Green, M. B. Kennel, J. F. Thomas & F. T. Connolly.** A simple model for cyclic variations in a spark-ignition engine, *SAE Technical Papers*, 962086, 1996.

[15] **N. H. Packard, J. P. Crutchfield, J. D. Farmer, R. S. Shaw.** Geometry from a time series, *Physical Review Letters*, 45 (9), 712-716, 1980.

[16] **H. D. I. Abarbanel, R. Brown, J. J. Sidorowich, L. Sh. Tsimring.** The analysis of observed chaotic data in physical systems, *Review of Modern Physics*, 65 (4), 1331-1388, 1993.

[17] **D. S. Broomhead, G. P. King.** Extracting qualitative dynamics from experimental data, *Physica D*, 20, 217-236, 1986.

[18] **J.F.Gibson, J. D. Farmer, M. Casdagli, S. Eubank.** An analytic approach to practical state space reconstruction, *Physica D*, 57, 1-30, 1992.

[19] **E. A. Jackson.** *Perspective of nonlinear dynamics*, Vol. 1, Cambridge University Press, 1992.

[20] **R. Borghi & M. Destriau.** *La combustion et les flammes*, Ed. Technip, Paris, 1995.

[21] **M. B. Young.** Cyclic dispersion in the homogeneous charge spark-ignition engine - A literature survey, *SAE Technical Paper Series*, 810020, 1981.